Int. J. Heat Mass Transfer. Vol. 36, No. 11, pp. 2827–2835, 1993
Printed in Great Britain

0017–9310/93 $6.00 + 0.00

Multicomponent droplet evaporation at intermediate Reynolds numbers

M. RENKSIZBULUT† and M. BUSSMANN
University of Waterloo, Mechanical Engineering Department, Waterloo, Ontario, Canada N2L 3G1

(*Received* 7 *July* 1992 *and in final form* 19 *November* 1992)

Abstract—The convective evaporation of a binary hydrocarbon droplet (decane–hexadecane) in air at 1000 K and at a pressure of 10 atmospheres has been studied using numerical methods. All transient effects including droplet size and velocity variations, heat and mass transfer within the liquid phase, and thermophysical property variations with temperature and concentration in both phases are included in the analysis. As the rate controlling process, liquid phase mass transfer is examined in detail. It is demonstrated that the existing drag coefficient, Sherwood number, and Nusselt number correlations originally developed for single-component droplets can be used for multicomponent droplets as well.

INTRODUCTION

MOST CONVENTIONAL hydrocarbon fuels used in power generation are miscible multicomponent liquids. Sprays are extensively employed as a practical means of dispersing such fuels in the oxidizer which is normally air. An understanding of the behavior of multicomponent droplets in air is therefore fundamental to the understanding and modeling of spray evaporation and combustion processes. High pressures and liquid injection velocities commonly encountered in combustion engines, such as gas turbines, dictate that the droplet lifetimes are spent in a highly convective environment. The intermediate Reynolds number flow ($Re = O(100)$) around the droplets influences not only the gas phase heat and mass transfer characteristics, but also initiates a circulatory motion within the droplet, which affects the nature of liquid phase heating and mass transfer.

Multicomponent droplet vaporization is poorly described by a batch-distillation type model [1] because fuel components do not necessarily vaporize sequentially from the most to the least volatile. Rather, more volatile fuel components may remain within the droplet core while less volatile components vaporize because liquid phase mass diffusion occurs very slowly, and resists the flux of more volatile components to the surface. Vaporization is then governed not only by component volatility, but also by the rate of species diffusion and droplet surface regression, as well as the nature of fluid motion within the droplet.

The presence of volatile components in the droplet interior also leads to the possibility of a so-called micro-explosion. As the more volatile components are depleted from the surface, they are not replenished immediately from the droplet interior due to the slowness of the mass diffusion process. Consequently, the less volatile components remaining at the surface cause an increase in the surface temperature. Theoretical work by Law [1] showed that, as a two-component droplet evaporates in a quiescent environment, the temperature within the droplet at a location rich in the volatile, low boiling point component may exceed the limit of superheat of the local mixture. Homogeneous nucleation occurs and the local mixture gasifies, causing droplet fragmentation or micro-explosion. This has also been observed experimentally by many researchers; for example, Lasheras *et al.* [2] and Wang *et al.* [3].

LITERATURE REVIEW

The following literature review focuses specifically on studies involving multicomponent droplets; from the classical spherically symmetric problem to convective droplet evaporation. Existing literature on single-component droplet vaporization and combustion have been reviewed in detail by Law [4], Sirignano [5], Faeth [6] and Dwyer [7], and therefore, will not be repeated here.

Landis and Mills [8] were first to examine the effects of mass transfer resistance within an evaporating multicomponent droplet. The spherically symmetric evaporation of a heptane–octane droplet in air (p^*_∞ = 1 atm, $T^*_\infty = 2300$ K, $Le_l = 18$) was studied using numerical methods. They concluded that evaporation is initially transient as the more volatile heptane is preferentially vaporized. While this causes a concentration gradient to develop, low mass diffusivity strongly resists the flux of heptane from the droplet core to replenish the surface layer. Species concentration profiles become essentially invariant, and the evaporation process attains a quasi-steady character. For the remainder of the lifetime, both com-

† Author to whom correspondence should be addressed.

NOMENCLATURE

B_H heat transfer number, $c^*_{p,g}(T^*_\infty - T^*_s)/L^*_s$
B_M mass transfer number, $(\Sigma_{i=1}^{F} Y_{i,s} - \Sigma_{i=1}^{F} Y_{i,\infty})/(1 - \Sigma_{i=1}^{F} Y_{i,s})$
c_p specific heat at constant pressure, $c^*_p/c^*_{p,\infty}$
C_D total drag coefficient, $C_D = C_F + C_P + C_T$
C_F friction drag coefficient, $2F^*_F/(\rho^*_\infty v^{*2}_\infty \pi R^{*2})$
C_P pressure drag coefficient, $2F^*_P/(\rho^*_\infty v^{*2}_\infty \pi R^{*2})$
C_T thrust coefficient, $2F^*_T/(\rho^*_\infty v^{*2}_\infty \pi R^{*2})$
D binary mass diffusion coefficient, D^*/D^*_∞
F^* force
h^*_H heat transfer coefficient
h^*_M mass transfer coefficient
k thermal conductivity, k^*/k^*_∞
L_v latent heat of vaporization, $L^*_v/(c^*_{p,\gamma} T^*_\gamma)$
Le Lewis number, $k^*/(\rho^* c^*_p D^*)$
$\dot{m}''$ mass flux, $\dot{m}''^*/(\rho^*_\infty v^*_{\infty,0})$
M^* molecular weight
Nu Nusselt number, $2R^* h^*_H/k^*$
p^*_i vapour pressure of species i
p pressure, $(p^* - p^*_\gamma)/(\rho^*_\infty v^{*2}_{\infty,0})$
Pe_H heat transfer Peclet number, $Re\ Pr$
Pe_M mass transfer Peclet number, $Re\ Sc$
Pr Prandtl number, $\mu^* c^*_p/k^*$
Q^* heat transfer rate
r radial coordinate, r^*/R^*
R instantaneous droplet radius, R^*/R^*_0
Re Reynolds number, $2R^* \rho^* v^*_\infty/\mu^*$
Re_m Reynolds number, $2R^* \rho^*_\infty v^*_\infty/\mu^*_l$
Sh Sherwood number, $2R^* h^*_M/(\rho^* D^*)$
Sc Schmidt number, $\mu^*/(\rho^* D^*)$
t time, $t^* v^*_{\infty,0}/R^*_0$
T temperature, T^*/T^*_∞
v_r radial velocity component, v^*_r/v^*_∞
v_θ tangential velocity component, v^*_θ/v^*_∞
v^*_∞ instantaneous free-stream velocity
V nondimensional free-stream velocity, $v^*_\infty/v^*_{\infty,0}$
X_i mole fraction of species i
Y_i mass fraction of species i, $X_i M^*_i/\Sigma_{i=1}^{n} X_i M^*_i$.

Greek symbols
α^* thermal diffusivity, $k^*/(\rho^* c^*_p)$
θ tangential coordinate
μ viscosity, μ^*/μ^*_∞
ρ density, ρ^*/ρ^*_∞
$\tau_{r\theta}$ shear stress, $\tau^*_{r\theta}/(\mu^*_\infty v^*_{\infty}/R^*)$
τ_{rr} normal stress, $\tau^*_{rr}/(\mu^*_\infty v^*_\infty/R^*)$.

Subscripts and superscripts
bp boiling point
f film conditions
F fuel component
g gas phase
H heat transfer
i species index
l liquid phase
m mixture
M mass transfer
n number of species
o initial conditions
s at the droplet surface
vc vortex center
θ local
∞ free-stream conditions
* dimensional quantity
$\wedge$ unit vector
$\rightarrow$ vector
$\sim$ tensor
$-$ spatial average.

ponents evaporate at a rate nearly proportional to their initial concentrations, as would occur in the hypothetical limit of zero diffusivity or infinite surface regression rate.

Law [1] studied the effect of liquid phase Lewis number on the spherically symmetric evaporation of a decane–dodecane droplet. For $Le_l = 30$, results were similar to those of Landis and Mills [8]. For $Le_l = 10$, evaporation no longer occurred as at the zero diffusivity limit; the core concentration of decane slowly decreased, and the surface concentration profile was less steep, and temporally varying. For $Le_l = 1$, concentrations within the droplet were nearly spatially uniform throughout the droplet lifetime, as vaporization approached the limit of batch distillation.

Lasheras *et al.* [2] investigated the possibility of micro-explosion for a variety of binary n-paraffin droplets burning at atmospheric pressure, at $Re \approx 0$. Micro-explosion was observed only for fuel mixtures of a certain minimum volatility difference, and then only for a certain range of concentrations. They were able to adequately predict the minimum concentration of the more volatile component for which disruption would occur, by equating the boiling point temperature of the less volatile component to the limit of superheat of the initial droplet mixture.

Randolph *et al.* [9] examined variations in average liquid phase species concentration by sampling two-component droplets vaporizing at $Re \approx 0$. Fuel component concentrations never reached steady values even for burning droplets, and varied much more during the lifetime of an evaporating droplet. The

average concentration of the more volatile component decreased more quickly as the difference between component volatility increased, and as lighter mixtures were examined. The observations were consistent with the estimated values of liquid mass diffusivity such that greater temporal variations in concentration corresponded to larger values of D_l^*.

Although the $Re \cong 0$ studies cited above provide much insight into the nature of mass transfer within multicomponent droplets, the extension to convective droplet vaporization introduces further complexities. In particular, the internal motion induced by shear at the surface alters the nature of heat and mass transfer in the liquid phase.

Lara-Urbaneja and Sirignano [10] examined the convective evaporation of binary fuel droplets, at $Re \sim 200$, 10 atm, and 1000 K. They modeled liquid phase heat and mass transfer as transient processes and assumed all other transport processes to be quasi-steady. The model involved an inviscid free-stream, gas and liquid phase boundary layers around the droplet surface, and an inviscid toroidal vortex in the droplet core. In spite of internal circulation, species concentrations were far from uniform, and component vaporization did not proceed sequentially. Rather, mass transport from the vortex center to the droplet surface occurred as diffusion across vortex streamlines of uniform concentration. The mass fraction at the vortex center remained near its initial value for the entire lifetime. The reduction in the characteristic diffusion time due to internal circulation was offset by a similar reduction in droplet lifetime. Consequently, mass transfer remained a transient process in spite of forced convective effects.

Lerner [11] performed experiments with heptane–dodecane droplets, undergoing convective evaporation at $Re \sim 100$, at low temperatures and at atmospheric pressure. The investigation covered only the early portion of the droplet lifetime. Droplet sampling revealed average concentrations between those predicted by the rapid-mixing and pure-diffusion models.

Tong and Sirignano [12] simplified the model of Lara-Urbaneja and Sirignano [10], combining a liquid phase vortex model with a one-dimensional gas phase model. The results were intermediate to those generated by limiting models (rapid-mixing and pure-diffusion) but closer to the predictions of the pure-diffusion model. The results of all three models were also compared with the experimental data of Lerner [11]. The comparison proved inconclusive, as both the vortex model and the spherical diffusion model predictions were within the uncertainty limits of the experimental data.

Megaridis and Sirignano [13] studied the convective evaporation of multicomponent droplets in order to determine the effects of initial droplet composition, ambient temperature, Reynolds number, and volatility differential. They found that a binary droplet with a higher initial concentration of the less volatile species had a shorter lifetime due to higher liquid heating rates. In order to compare the effects of volatility differential, the case of a 50% decane–50% benzene (by mass) droplet vs a 50% octane–50% benzene droplet was studied. They observed that the larger volatility differential of the decane–benzene droplet manifested itself in a more pronounced preferential vaporization of the more volatile benzene, and that there was a high likelihood of micro-explosion in the decane–benzene droplet, while there was no possibility of micro-explosion in the octane–benzene droplet.

An experimental investigation by Yap *et al.* [14] of the convective combustion of hexane–hexadecane droplets, at $Re \sim 20$–40, clearly demonstrated the occurrence of micro-explosions. The results were compared with those of Lasheras *et al.* [2], of similar droplets burning at $Re \approx 0$. Droplets in the convective environment exploded in a quarter of the time but the droplet diameters at disruption were essentially equal in both studies.

The following sections provide the results of a numerical study involving the transient convective evaporation of a decane–hexadecane droplet in air. The present work focuses on characterizing, in detail, the effects of gas and liquid phase transients, and variable thermophysical properties on the associated heat, mass and momentum transfer processes. Predictions of the drag coefficient, Nusselt and Sherwood numbers, and comparisons to existing correlations are also presented. Such correlations are essential requirements in spray modeling.

FORMULATION

The mathematical model is based on the following assumptions: (1) the droplet remains spherical at all times; (2) the gas and liquid flow fields are laminar and axisymmetric; (3) the liquid phase mixture is ideal; (4) the two phases at the droplet surface are in thermodynamic equilibrium and are related by Raoult's law; (5) air is insoluble in the liquid phase; (6) effects due to external body forces, thermal radiation, and viscous dissipation are negligible; (7) the Soret and Dufour effects, and pressure diffusion are negligible; and (8) mass diffusion in both phases obeys Fick's law. The ambient air is taken to be quiescent, and the motion of the droplet is observed from a frame of reference attached to the droplet. Table 1 contains the equations which represent the conservation of mass, momentum, energy and species, cast in spherical coordinates and non-dimensionalized as given in the Nomenclature section. Table 2 provides the associated boundary conditions.

Overall conservation of mass and momentum results in the following equations for the droplet surface regression rate $\mathrm{d}R/\mathrm{d}t$, and the droplet deceleration $\mathrm{d}V/\mathrm{d}t$ due to drag:

$$\frac{\mathrm{d}R}{\mathrm{d}t} = -\frac{1}{2\bar{\rho}_l}\left(\int_0^{\pi} \dot{m}''_\theta \sin\theta \,\mathrm{d}\theta + \tfrac{2}{3}R\frac{\mathrm{d}\bar{\rho}_l}{\mathrm{d}t}\right) \quad (12)$$

Table 1. The governing equations

$$\frac{\partial}{\partial t}(\rho V R\phi)+V^2\vec{\nabla}\cdot\left\{\rho\phi\left[\left(v_r-\frac{r}{V}\frac{dR}{dt}\right)\hat{r}+v_\theta\hat{\theta}\right]\right\}=\frac{V}{T}\vec{\nabla}\cdot(\Gamma_\phi\vec{\nabla}\phi)+S_\phi \tag{1}$$

Equation	ϕ	Γ_ϕ	S_ϕ
Continuity	1	0	S_C
Radial momentum	v_r	$2\mu/Re_{\infty,0}$	S_{RM}
Tangential momentum	v_θ	$2\mu/Re_{\infty,0}$	S_{TM}
Energy	T	$2k/(c_p Re_{\infty,0} Pr_\infty)$	S_E
Species	Y_i	$2\rho D_{i,m}/(Re_{\infty,0} Sc_\infty)$	S_Y

$$S_C=\rho R\frac{dV}{dt}-2\rho V\frac{dR}{dt}$$

$$S_{RM}=V^2[\vec{\nabla}\cdot(\rho\vec{v}v_r)-\vec{\nabla}\cdot(\rho\vec{v}\vec{v})_r]-\frac{2V}{Re_{\infty,0}R}[\vec{\nabla}\cdot\mu\vec{\nabla}v_r-(\vec{\nabla}\cdot\vec{\tau})_r]-2\rho Vv_r\frac{dR}{dt}-\frac{\partial p}{\partial r}-\rho R\cos\theta\frac{dV}{dt}$$

$$S_{TM}=V^2[\vec{\nabla}\cdot(\rho\vec{v}v_\theta)-\vec{\nabla}\cdot(\rho\vec{v}\vec{v})_\theta]-\frac{2V}{Re_{\infty,0}R}[\vec{\nabla}\cdot\mu\vec{\nabla}v_\theta-(\vec{\nabla}\cdot\vec{\tau})_\theta]-2\rho Vv_\theta\frac{dR}{dt}-\frac{1}{r}\frac{\partial p}{\partial\theta}+\rho R\sin\theta\frac{dV}{dt}$$

$$S_E=\rho TR\frac{dV}{dt}-2\rho TV\frac{dR}{dt}+\frac{2V}{Re_{\infty,0}Pr_\infty R}\frac{k}{c_p^2}(\vec{\nabla}T\cdot\vec{\nabla}c_p)+\frac{2\rho V}{Sc_\infty Re_p}\left(\vec{\nabla}T\cdot\sum_{i=1}^{n}c_{pi}D_{i,m}\vec{\nabla}Y_i\right)$$

$$S_Y=\rho Y_iR\frac{dV}{dt}-2\rho Y_iV\frac{dR}{dt}$$

Table 2. The boundary conditions

- Gas/liquid interface ($r=1,\ 0\leqslant\theta\leqslant\pi$)

$$T_l=T_g;\quad v_{\theta,l}=v_{\theta,g} \tag{2}$$

$$\left(-k\frac{\partial T}{\partial r}\right)_l=\left(-k\frac{\partial T}{\partial r}\right)_g+\tfrac{1}{2}Re_{\infty,0}Pr_\infty R\dot{m}''_\theta L_s \tag{3}$$

$$\dot{m}''_\theta Y_{i,l}-\frac{2\rho_l D_{i,m,l}}{Re_{\infty,0}Sc_\infty R}\left(\frac{\partial Y_i}{\partial r}\right)_l=\dot{m}''_\theta Y_{i,g}-\frac{2\rho_g D_{i,m,g}}{Re_{\infty,0}Sc_\infty R}\left(\frac{\partial Y_i}{\partial r}\right)_g \tag{4}$$

$$X_{i,g}=X_{i,l}X^o_{i,g}\quad\text{where}\quad X^o_{i,g}=p_i^*(T^*)/p^*_\infty \tag{5}$$

$$v_{r,l}=\frac{1}{V}\left(\frac{\dot{m}''_\theta}{\rho_l}+\frac{dR}{dt}\right);\quad v_{r,g}=\frac{1}{V}\left(\frac{\dot{m}''_\theta}{\rho_g}+\frac{dR}{dt}\right) \tag{6}$$

$$\mu_l\left(\frac{\partial v_\theta}{\partial r}-\frac{v_\theta}{r}+\frac{1}{r}\frac{\partial v_r}{\partial\theta}\right)_l=\mu_g\left(\frac{\partial v_\theta}{\partial r}-\frac{v_\theta}{r}+\frac{1}{r}\frac{\partial v_r}{\partial\theta}\right)_g \tag{7}$$

- Free-stream inlet ($r=\infty,\ 0\leqslant\theta\leqslant\pi/2$)

$$T=1;\quad Y_i=0;\quad v_r=-\cos\theta;\quad v_\theta=\sin\theta. \tag{8}$$

- Free-stream outlet ($r=\infty,\ \pi/2\leqslant\theta\leqslant\pi$)

$$\frac{\partial\phi}{\partial r}=0\quad\text{where}\quad\phi=v_r,v_\theta,T,Y_i. \tag{9}$$

- Axis of symmetry ($0\leqslant r\leqslant\infty,\ \theta=0,\pi$)

$$v_\theta=0;\quad\frac{\partial\phi}{\partial\theta}=0\quad\text{where}\quad\phi=v_r,T,Y_i. \tag{10}$$

- Origin ($r=0$)

$$\left(\frac{\partial\phi}{\partial r}\right)_{\theta=\pi/2}=0\quad\text{where}\quad\phi=v_r,v_\theta,T,Y_i. \tag{11}$$

$$\frac{dV}{dt}=-\frac{3}{8}\frac{C_DV^2}{\bar{\rho}_lR}. \tag{13}$$

$$C_F=\frac{8}{Re_{\infty,0}RV}\int_0^\pi(\tau_{r\theta}\sin\theta-\tau_{rr}\cos\theta)_s\sin\theta\,d\theta \tag{14}$$

The total drag coefficient C_D is the sum of the contributions arising from friction drag C_F, pressure drag C_P, and asymmetrical blowing due to evaporation C_T

$$C_P=\frac{4}{V^2}\int_0^\pi p_s\cos\theta\sin\theta\,d\theta \tag{15}$$

$$C_T = 2\int_0^{\pi} \rho_g (v_r^2 \sin 2\theta - 2v_r v_\theta \sin^2\theta)_s \, d\theta. \quad (16)$$

The surface-averaged Nusselt and Sherwood numbers are given by

$$Nu_\infty = \frac{1}{2}\int_0^{\pi} \left(\frac{2k_g}{1-T}\frac{\partial T}{\partial r}\right)_{s,\theta} \sin\theta \, d\theta \quad (17)$$

$$Sh_\infty = \frac{1}{2}\int_0^{\pi} \left(\frac{2\rho_g D_{i,m}}{Y_{i,\infty} - Y_i}\frac{\partial Y_i}{\partial r}\right)_{s,\theta} \sin\theta \, d\theta. \quad (18)$$

In order to solve the governing equations, a numerical method based on a conservative control-volume technique was employed. In this procedure, the integration of equation (1) (see Table 1) over a finite-volume in the calculation domain, and over time yields a system of linearized equations of the form

$$a_P\phi_P = a_N\phi_N + a_E\phi_E + a_S\phi_S + a_W\phi_W + b_P \quad (19)$$

which relate the value of a variable ϕ at a point P to its values at the four neighboring control volumes. N, S, E and W label grid points to the North, South, East and West of the control volume centered at P. In the present work, the spherical numerical grid consisted of 45 control volumes tangentially spaced 4° apart, and 70 radial control volumes (20 in the liquid phase and 50 in the gas phase), unevenly distributed to provide high spatial resolution at the liquid–gas interface. The grid extended outward in the gas phase to 40 droplet radii, where the free-stream boundary conditions given in Table 2 were invoked. The application of equation (19) to all control-volumes results in coupled (through the coefficients a_i) systems of algebraic equations for the field variables v_r, v_θ, T, p and Y_i, which are then iteratively solved at every time-step. (The well known control-volume method is fully discussed in the *Handbook of Numerical Heat Transfer* [15].) The computer code has been extensively validated as discussed in Haywood *et al.* [16]. Further details of the present numerical treatment, and variable thermophysical property correlations are given in Bussmann [17].

RESULTS AND DISCUSSION

This section presents the results of a detailed examination of the convective evaporation of a decane–hexadecane droplet. The ambient air temperature and pressure are specified to be 1000 K and 10 atmospheres, respectively. Initially, the liquid phase is motionless at 300 K with a homogeneous species concentration of 50% decane–50% hexadecane by mass. The initial Reynolds number $Re_{\infty,o}$ is 100 which, for example, corresponds to a 100 μm diameter droplet injected at a relative velocity of 10 m s^{-1}.

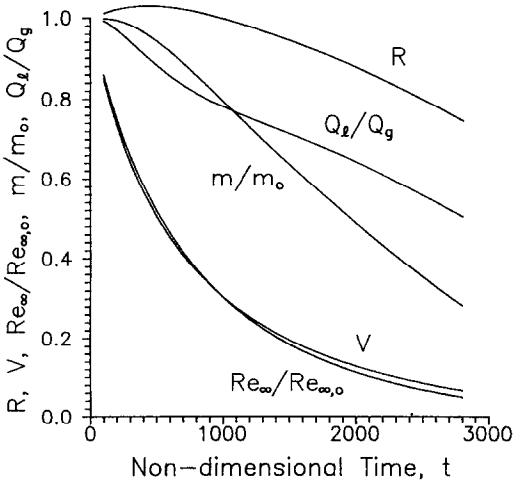

FIG. 1. Temporal histories of the droplet radius R, droplet velocity V, Reynolds number $Re_\infty/Re_{\infty,o}$, droplet mass m/m_o and, liquid heating fraction Q_l/Q_g.

Figure 1 shows the lifetime variations of the droplet radius R, droplet velocity V, Reynolds number $Re_\infty/Re_{\infty,o}$, droplet mass m/m_o, and the liquid heating fraction Q_l/Q_g. The high ambient pressure has a strong effect on the relative rates at which R and V vary. Droplet velocity decreases quickly and accounts for practically all of the decrease in Re_∞, while R varies little. The decrease in liquid density as the droplet heats up is significant such that following an initial period of thermal expansion, droplet size returns to $R = 1$ at $t = 1000$ after 20% of the mass has been vaporized. By that time, Re_∞ has been reduced to 30 by the decrease in V. Liquid heating is also a very important transient effect which persists for the entire lifetime. For example, even at $t = 2800$, when only 28% of droplet mass remains, liquid heating still accounts for 50% of the energy transferred to the surface. This is a consequence of the low volatility of the mixture, characterized especially by the higher boiling points of the components at 10 atmospheres.

Figure 2 shows the lifetime history of the total drag coefficient C_D, as well as the components C_P, C_F and C_T. As expected, the decrease with time of Reynolds number corresponds to an increase in C_D. Both pressure and friction drag contribute significantly to total drag, although as Reynolds number decreases, C_P gradually becomes larger than C_F, similar to flow around a solid sphere. The thrust coefficient C_T is negative and thus accelerates the droplet, but the effect is minor, as C_T decreases total drag by a maximum of 3.5%. The C_D trends observed by Megaridis and Sirignano [13] in their study of binary droplets are not found in the present work. Their results show an unexpected trend such that C_D first decreases as the Reynolds number decreases to about 65 from its initial value of 100, after which C_D begins to increase. Secondly, their results show very large reductions of over 50% in drag as compared to a solid sphere at the

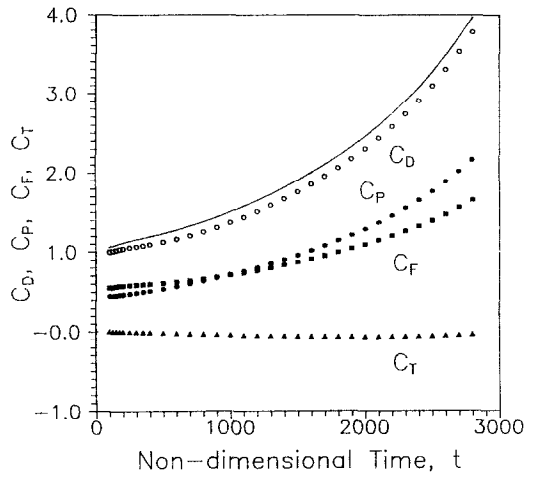

FIG. 2. Drag coefficients: total drag C_D, pressure drag C_P, friction drag C_F, thrust coefficient C_T; ——— equation (20); symbols represent the numerical data.

same Reynolds number. Such large reductions contradict the well-known experimental results of Yuen and Chen [18] which indicate that, on total drag, the net effect of blowing at the surface due to evaporation is small. While surface blowing causes a reduction in friction drag, it also causes an increase in pressure drag due to earlier flow separation. The net result is that surface blowing has a small effect on C_D.

Renksizbulut and Yuen [19] modified a solid sphere drag correlation to account for the effects of surface mass transfer and variable thermophysical properties, and Renksizbulut and Haywood [20] proposed a further modification to account for liquid phase heating

$$C_D(1+B'_{H,f})^{0.2} = \frac{24}{Re_m}(1+0.2Re_m^{0.63}); \quad 20 \leqslant Re_m \leqslant 300 \tag{20}$$

$$B'_{H,f} = \frac{c^*_{p,f}(T^*_\infty - T^*_s)}{L^*_s}\left(1-\frac{Q_l}{Q_g}\right). \tag{21}$$

As shown in Fig. 2, this correlation predicts the data well (within 10%). The slight over-prediction is the result of two factors. First, the motion of the droplet surface, which reduces velocity gradients and thereby friction drag, is unaccounted for in the drag correlation. Liquid motion is especially intense at higher ambient pressures, and for higher Reynolds numbers. For example, surface velocity, at $\theta = 90°$, rises to 15% of the free-stream velocity at $t = 800$, and even at $t = 2800$, surface velocity is still 7% of the free-stream velocity. Secondly, the drag correlation, as indicated, has a lower Reynolds number limit of 20. Near the end of the lifetime, at $t = 2800$, the Reynolds number is about 8.

Like the correlation for total drag, Renksizbulut and Yuen [21] modified a solid sphere Nusselt number correlation to account for the effects of surface mass transfer, variable thermophysical properties and liquid heating

$$Nu_f(1+B'_{H,f})^{0.7} = 2+0.57Re_m^{1/2}Pr_f^{1/3}; \quad 20 \leqslant Re_m \leqslant 2000. \tag{22}$$

As shown in Fig. 3, Nusselt number is predicted very well. The correlation begins to over-predict Nusselt number by about 14% only as the Reynolds number decreases below the range suggested for the correlation.

Renksizbulut *et al.* [22] also proposed a gas phase Sherwood number correlation based on numerical and experimental data of evaporating single-component droplets. This correlation, which accounts for surface mass transfer, variable thermophysical properties and liquid heating, may also be applied to the multicomponent case as given below

$$Sh_{i,f}(1+B_M)^{0.7} = 2+0.87Re_m^{1/2}Sc_f^{1/3}; \quad 20 \leqslant Re_m \leqslant 2000 \tag{23}$$

$$B_M = \frac{\Sigma_{i-1}^{I} Y_{i,s} - \Sigma_{i-1}^{I} Y_{i,\infty}}{1-\Sigma_{i-1}^{I} Y_{i,s}} \tag{24}$$

where the B_M definition covers all species present in the liquid phase. Figure 4 shows the good agreement (within 18%) between the actual and correlated $Sh_{i,f}$ for decane and hexadecane. The correlation is more accurate in its predictions for the predominantly vaporizing fuel component. When decane is vaporized preferentially, early in the lifetime, the correlation more accurately predicts $Sh_{C_{10}H_{22},f}$. Then, as the surface concentration of decane decreases, and hexadecane is vaporized preferentially, the correlation for $Sh_{C_{16}H_{34},f}$ provides a better agreement.

The focus of this section now turns to liquid phase processes, and the nature of multicomponent vaporization, as presented in Figs. 5–10. Figure 5 shows temporal histories of surface, vortex center, and average droplet temperatures; Fig. 6 histories of surface,

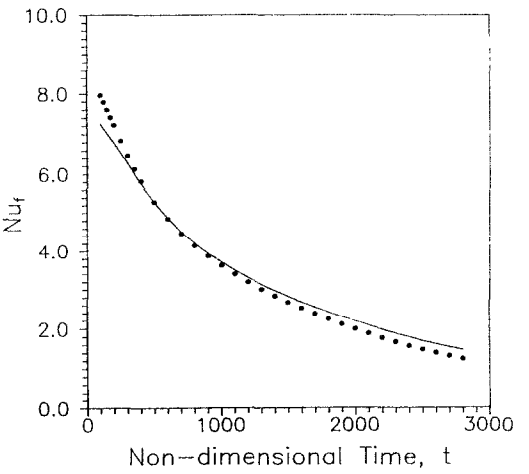

FIG. 3. Temporal history of Nusselt number; ● numerical data; ——— equation (22).

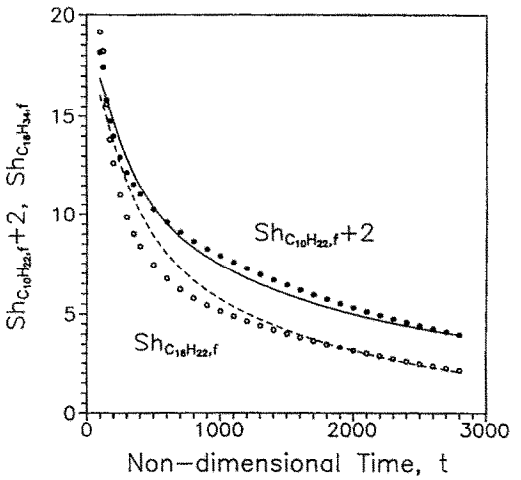

FIG. 4. Temporal histories of gas phase Sherwood numbers $Sh_{i,f}$ for $C_{10}H_{22}$ and $C_{16}H_{34}$; ● ○ numerical data; dashed and solid lines represent equation (23).

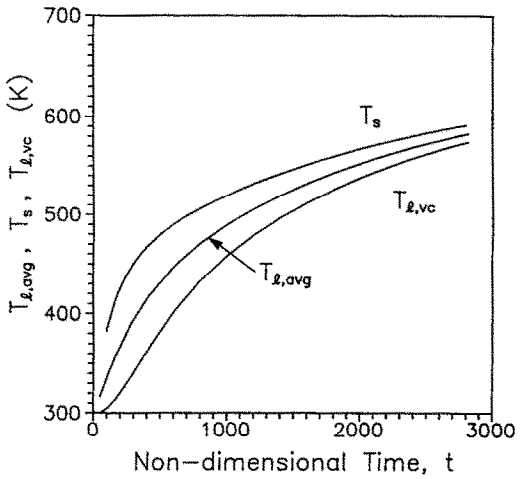

FIG. 5. Temporal histories of surface, vortex center, and average liquid temperatures.

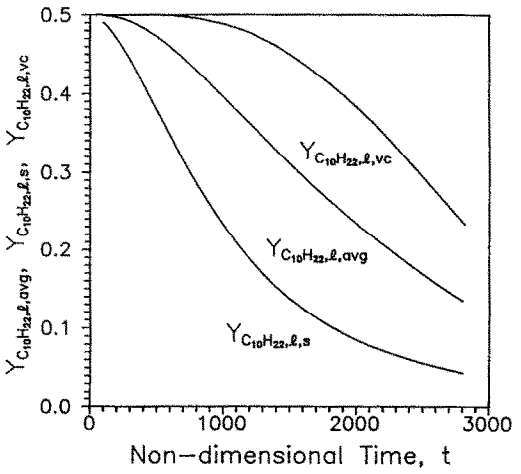

FIG. 6. Temporal histories of surface, vortex center, and average liquid decane concentrations.

vortex center, and average decane concentration in the liquid phase; Fig. 7 histories of fuel vapour concentrations at the droplet surface; Fig. 8 component and total mass transfer rates; and Figs. 9 and 10 liquid

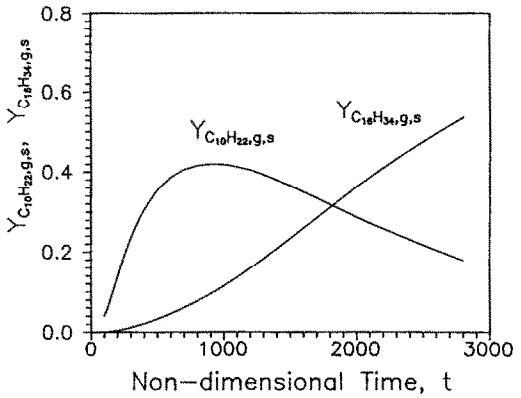

FIG. 7. Temporal histories of gas phase concentrations of decane and hexadecane at the droplet surface.

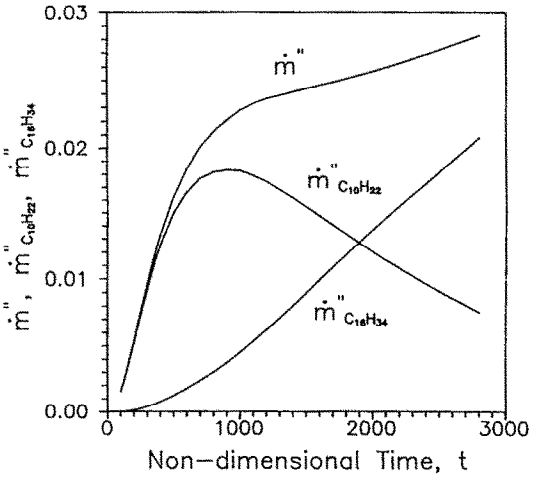

FIG. 8. Temporal histories of component and total mass transfer rates.

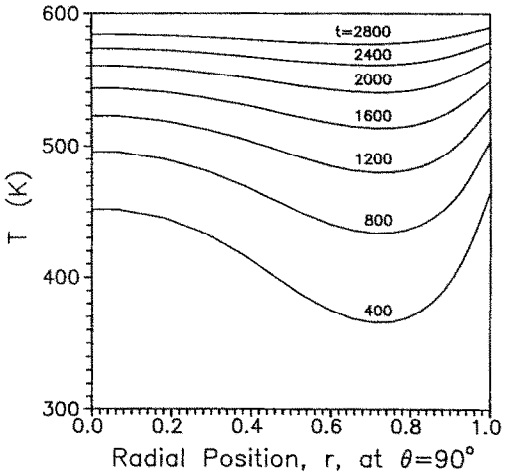

FIG. 9. Temporal history of the radial liquid temperature profile at $\theta = 90°$.

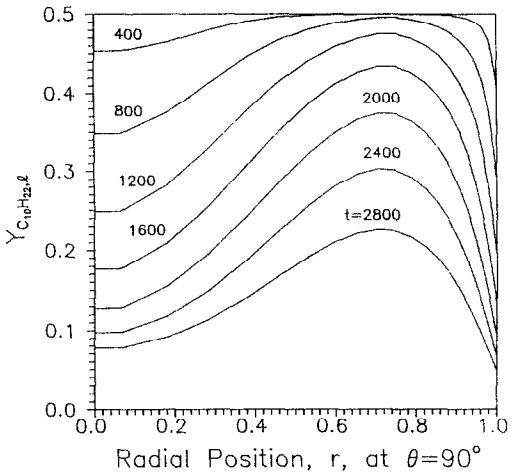

FIG. 10. Temporal history of the radial concentration profile of decane within the droplet at $\theta = 90°$.

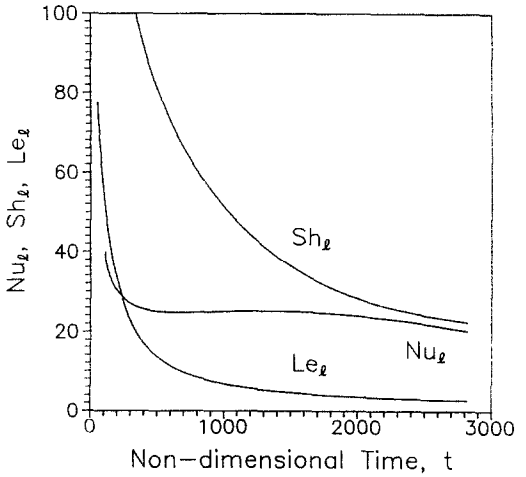

FIG. 11. Temporal histories of liquid phase Nusselt Nu_l, Sherwood Sh_l, and Lewis numbers Le_l.

temperature and concentration profiles at $\theta = 90°$. Collectively, these figures produce the following physical picture.

Evaporation begins with the preferential vaporization of decane from the surface, and the development of a vortex within the droplet. A steep concentration profile develops, from the vortex center, at the initial concentration, to the droplet surface which becomes progressively richer in the less volatile hexadecane (Fig. 10). Mass diffusivity is small and little decane diffuses across the vortex streamlines to the surface. Concurrently, the droplet surface temperature rises quickly, and the droplet interior begins to heat up (Fig. 5). Component vapor pressures and mass transfer rates increase. Surface temperature increases throughout the lifetime, driven higher by the increasing surface concentration of the less volatile hexadecane. As the liquid temperature rises, the mass diffusivity increases and at $t \approx 600$, the decane concentration in the vortex center begins to decrease (Fig. 6). However, the diffusion of decane from the vortex center to the droplet surface is not fast enough to replenish all of the decane which is evaporating. By $t = 1000$, the surface concentration of decane is so low that in spite of increasing droplet surface temperature, the mass flux of decane begins to decrease (Fig. 8). In contrast, the mass flow of hexadecane increases steadily throughout the droplet life. Near the end of the droplet life, the liquid surface mass fraction of decane has been reduced to less than 0.05 (Fig. 6), yet the vaporization of decane still accounts for over 25% of the total mass flux (Fig. 8).

To account for the changing liquid temperature and concentration, liquid mass diffusivity was correlated by $D_l^* \sim T^*/\mu_l^*$, as recommended by Reid *et al.* [23]. For the liquid temperatures encountered in this study, D_l^* increased by more than one order of magnitude. Considering that the liquid thermal diffusivity α_l^* decreases with increasing temperature, Le_l decreased by a factor of 30 over the droplet lifetime. Near the end of the lifetime, with liquid temperature near 600 K, $Le_l \approx 3$ (Fig. 11). Clearly, to regard D_l^* or Le_l as constant is to disregard an important transient effect. Furthermore, to assume D_l^* to be negligible and to model mass diffusion by the zero diffusivity limit is to disregard the effect of temperature, and the large liquid temperature changes which occur during the vaporization of heavy hydrocarbons, especially at high ambient pressures. Randolph *et al.* [9] point out that previous attempts at modeling multicomponent vaporization may have assumed values of Le_l which were too high, and that lower values of Le_l led to better predictions of their experimental data. The variation of D_l^* with temperature will also affect the possibility of micro-explosion. The boiling point and consequently the droplet temperature increase with ambient pressure. However, the limit of superheat varies little, unless the pressure approaches the critical value of the mixture. Thus, micro-explosion should occur more readily at higher pressures. This enhancement, however, will be tempered by a higher liquid temperature, and mass diffusivity, which will allow greater vaporization of more volatile components. In turn, the droplet mixture will become less volatile, and the limit of superheat will increase.

Based on work by Johns and Beckmann [24], Haywood *et al.* [16] proposed a liquid Nusselt number based on the difference between the droplet surface temperature T_s^* and average liquid temperature $\bar{T}_l^*$ such that

$$Nu_l = \frac{1}{2\bar{k}_l} \int_0^{\pi} \left(\frac{2\bar{k}_l}{\bar{T}_s - \bar{T}_l} \frac{\partial T}{\partial r} \right)_{s,\theta,t} \sin\theta \, d\theta. \quad (25)$$

Their study of the convective evaporation of a single component (heptane) droplet at atmospheric pressure revealed that, following a short period of adjustment, $Nu_l \to 22$. This is a valuable result, for when it applies, it provides a relatively simple means of modeling liquid heating [25]. Figure 11 shows a similar variation

of Nu_l for the multicomponent droplet. Similar to Nu_l, a Sh_l may be defined to characterize liquid phase mass transfer

$$Sh_l = \frac{1}{2\overline{\rho_l D_l}} \int_0^\pi \left(\frac{2\overline{\rho_l D_l}}{\bar{Y}_{i,s} - \bar{Y}_{i,l}} \frac{\partial Y_i}{\partial r} \right)_{s,\theta,l} \sin\theta \, d\theta. \quad (26)$$

Figure 11 shows that Sh_l approaches a similar limit to Nu_l, but much more slowly, as the time for development of a quasi-steady profile varies as $1/D_l^*$ vs $1/\alpha_l^*$ for Nu_l.

CONCLUSIONS

The following conclusions emerge from the results of the present work.

- At elevated pressures, the evaporation of relatively heavy hydrocarbon droplets is essentially controlled by liquid phase heating which persists throughout the droplet lifetime. The Reynolds number decreases largely due to the deceleration of the droplet, as droplet radius varies much more slowly because of the relatively low volatilities of the fuel components.
- Quasi-steady applications of existing correlations for the drag coefficient, and Nusselt and Sherwood numbers provide accurate predictions of heat, mass, and momentum transfer rates associated with multicomponent droplet evaporation at intermediate Reynolds numbers. This is an important observation because current spray models rely on such correlations to interface the continuous and dispersed phases.
- Mass transfer within the liquid phase is a highly transient phenomenon. The diffusion of liquid species is the slowest process associated with multicomponent droplet evaporation. An important aspect of mass diffusion in the liquid phase is the variation of mass diffusivity D_l^* with temperature. For heavy hydrocarbons, D_l^* may increase by an order of magnitude during the droplet lifetime. In the present work, the liquid phase Lewis number decreased by a factor of 30. Hence, the commonly used constant Lewis number assumption is not a realistic one.

Acknowledgement—This research was financially supported by the Natural Sciences and Engineeering Research Council of Canada. The authors also acknowledge the assistance of David Leppinen, an undergraduate student, during the preparation of the manuscript.

REFERENCES

1. C. K. Law, Internal boiling and superheating in vaporizing multicomponent droplets, *A.I.Ch.E. Jl* **24**(4), 626–632 (1978).
2. J. C. Lasheras, A. C. Fernandez-Pello and F. L. Dryer, Experimental observations on the disruptive combustion of free droplets of multicomponent fuels, *Combust. Sci. Technol.* **22**, 195–209 (1980).
3. C. H. Wang, X. Q. Liu and C. K. Law, Combustion and microexplosion of freely falling multicomponent droplets, *Combust. Flame* **56**, 175–197 (1984).
4. C. K. Law, Recent advances in droplet vaporization and combustion, *Prog. Energy Combust. Sci.* **8**, 171–201 (1982).
5. W. A. Sirignano, Fuel droplet vaporization and spray combustion theory, *Prog. Energy Combust. Sci.* **9**, 291–322 (1983).
6. G. M. Faeth, Evaporation and combustion of sprays, *Prog. Energy Combust. Sci.* **9**, 1–76 (1983).
7. H. A. Dwyer, Calculation of droplet dynamics in high temperature environments, *Prog. Energy Combust. Sci.* **15**, 131–158 (1989).
8. R. B. Landis and A. F. Mills, Effect of internal diffusion resistance on the evaporation of binary droplets, *Fifth Int. Heat Transfer Conf.*, Tokyo, Paper B7-9 (1974).
9. A. L. Randolph, A. Makino and C. K. Law, Liquid-phase diffusional resistance in multicomponent droplet gasification, *Twenty-first Symp. (Int.) Combustion*, The Combustion Institute, pp. 601–608 (1986).
10. P. Lara-Urbaneja and W. A. Sirignano, Theory of transient multicomponent droplet vaporization in a convective field gasification, *Eighteenth Symp. (Int.) Combustion*, The Combustion Institute, pp. 1365–1374 (1981).
11. S. L. Lerner, Multicomponent fuel droplet vaporization at large Reynolds numbers, Ph.D. Thesis, Princeton University, Princeton, New Jersey (1980).
12. A. Y. Tong and W. A. Sirignano, Multicomponent droplet vaporization in a high temperature gas, *ASME Winter Annual Meeting*, Paper 84-WA/HT-17 (1984).
13. C. M. Megaridis and W. A. Sirignano, Multicomponent droplet vaporization in a convecting environment. In *Heat and Mass Transfer in Fire and Combustion Systems* (Edited by W. L. Grosshandler and H. G. Semerjian), Publication HTD-148, pp. 71–79. ASME, New York (1990).
14. L. T. Yap, I. M. Kennedy and F. L. Dryer, Disruptive and micro-explosive combustion of free droplets in highly convective environments, *Combust. Sci. Technol.* **41**, 291–313 (1984).
15. W. J. Minkowycz, E. M. Sparrow, G. E. Schnieder and R. H. Plecher (Eds), *Handbook of Numerical Heat Transfer*, Chaps. 6 and 7. Wiley, New York (1988).
16. R. J. Haywood, R. Nafziger and M. Renksizbulut, A detailed examination of gas and liquid phase transient processes in convective droplet evaporation, *J. Heat Transfer* **111**(2), 495–502 (1989).
17. M. Bussmann, Studies on convective droplet evaporation, M.A.Sc. Thesis, University of Waterloo, Waterloo, Canada (1990).
18. M. C. Yuen and L. W. Chen, On drag of evaporating liquid droplets, *Combust. Sci. Technol.* **14**, 86–91 (1976).
19. M. Renksizbulut and M. C. Yuen, Numerical study of droplet evaporation in a high-temperature air stream, *J. Heat Transfer* **105**, 389–397 (1983).
20. M. Renksizbulut and R. J. Haywood, Transient droplet evaporation with variable properties and internal circulation at intermediate Reynolds numbers, *Int. J. Multiphase Flow* **14**(2), 189–202 (1988).
21. M. Renksizbulut and M. C. Yuen, Experimental study of droplet evaporation in a high-temperature air stream, *J. Heat Transfer* **105**, 384–388 (1983).
22. M. Renksizbulut, R. Nafziger and X. Li, A mass transfer correlation for droplet evaporation in high-temperature flows, *Chem. Engng Sci.* **46**(9), 2351–2358 (1991).
23. R. C. Reid, J. M. Prausnitz and B. E. Poling, *The Properties of Liquids and Gases*, 4th Edn, Chap. 11. McGraw-Hill, New York (1987).
24. L. E. Johns, Jr and R. B. Beckmann, Mechanism of dispersed-phase mass transfer in viscous, single-drop extraction systems, *A.I.Ch.E. Jl* **12**, 10–16 (1966).
25. M. Renksizbulut, M. Bussmann and X. Li, A droplet vaporization model for spray calculations, *Particle & Particle Systems Characterization* **9**, 59–65 (1992).